

Nanoparticle-Based CT Imaging Technique for Longitudinal and Quantitative Stem Cell Tracking within the Brain: Application in Neuropsychiatric Disorders

Oshra Betzer,^{†,§} Amit Schwartz,[‡] Menachem Motiei,[§] Gila Kazimirsky,[‡] Iris Gispan,[‡] Efrat Damti,[‡] Chaya Brodie,^{‡,⊥,||} Gal Yadid,^{†,‡,*} and Rachela Popovtzer^{§,⊥,*}

[†]Gonda Brain Research Center, Bar-Ilan University, Ramat-Gan 52900, Israel, [‡]Everard and Mina Goodman Faculty of Life Sciences, Bar-Ilan University, Ramat-Gan 52900, Israel, [§]Faculty of Engineering, Bar-Ilan University, Ramat-Gan 52900, Israel, [⊥]Institutes of Nanotechnology & Advanced Materials, Bar-Ilan University, Ramat-Gan 52900, Israel, and ^{||}Hermelin Brain Tumor Center, Department of Neurosurgery, Henry Ford Hospital, Detroit, Michigan 48202, United States

ABSTRACT A critical problem in the development and implementation of stem cell-based therapy is the lack of reliable, noninvasive means to image and trace the cells post-transplantation and evaluate their biodistribution, final fate, and functionality. In this study, we developed a gold nanoparticle-based CT imaging technique for longitudinal mesenchymal stem cell (MSC) tracking within the brain. We applied this technique for noninvasive monitoring of MSCs transplanted in a rat model for depression. Our research reveals that cell therapy is a potential approach for treating neuropsychiatric disorders. Our results, which demonstrate that cell migration could be detected as early as 24 h and up to one month post-transplantation, revealed that MSCs specifically navigated and homed to distinct depression-related brain regions. We further developed a noninvasive quantitative CT ruler, which can be used to determine the number of cells residing in a specific brain region, without tissue destruction or animal scarification. This technique may have a transformative effect on cellular therapy, both for basic research and clinical applications.



KEYWORDS: cell tracking · Mesenchymal stem cells (MSCs) · gold nanoparticles · CT · depression disorders

Stem cell-based therapy using mesenchymal stem cells (MSCs) has emerged as a novel and successful approach for the treatment of various brain pathologies, such as brain injury and stroke, multiple sclerosis (MS), Parkinson's disease and *amyotrophic lateral sclerosis (ALS)*.^{1–4} MSCs exhibit homing abilities to sites of lesion, injury, and inflammation;⁵ produce neurotropic factors; and exert anti-inflammatory effects.^{6,7} In addition, MSCs can promote endogenous neurogenesis⁸ and differentiate into neural-like cell types, and thus exert a prolonged regenerative effect.⁹ Yet, a critical problem in the development and implementation of cell-based therapy is lack of reliable means to image and trace the cells post-transplantation, and interpret their therapeutic outcomes. This leads to a deficiency in consistent and unbiased data on activity, distribution, and survival of stem cells *in vivo*.^{10,11} A recent meta-analysis of pre-clinical research revealed that despite the

potential efficacy of cell therapy for treating neurological disorders, no consensus exists regarding cell dosage, optimal route of delivery, cell migration and mechanisms underlying success or failure of treatment.¹² Furthermore, while the effectiveness of cell therapy for internal disorders, such as diabetes, liver failure, or myocardial infarction can be evaluated with comparatively objective measures and markers,^{13,14} neurological disorders are more challenging in this regard.¹⁵

There are several conservative approaches for tracking stem cells *in vivo*; however, the majority of these are destructive, necessitating scarification of the animals at various time points for biological identification and histology.¹⁶ Radionuclides have short half-lives, and thus are not ideal for long-term imaging studies.¹⁷ Reporter genes indirectly label cells and are not diluted by cell division, but they require the cells to be genetically manipulated, which could alter cell function,

* Address correspondence to yadidg@biu.ac.il, rachela.popovtzer@biu.ac.il.

Received for review June 10, 2014 and accepted August 18, 2014.

Published online August 18, 2014 10.1021/nn503131h

© 2014 American Chemical Society

and a substrate must be intravenously administered for each imaging session.¹⁸ Optical imaging is based on the penetration ability of light and, therefore, cannot be utilized for monitoring cells within deep brain structures.¹⁷ Recently, various types of nanoparticles have been suggested as contrast agents, mainly for MRI,¹⁹ and are expected to play a major role in the future of molecular imaging due to their many advantages over conventional contrast agents.

In the present work we demonstrate, for the first time, the development of a novel gold nanoparticle (GNP)-based CT imaging technique, for long-term cell tracking and imaging within the brain. We show that GNPs can be effectively loaded in human MSCs (hMSCs) pre-transplantation, without affecting cell viability or differentiation. As GNPs are ideal CT contrast agents,^{20–25} we were able to image and trace these MSCs both *in vivo* and *ex vivo* and evaluate their migration, biodistribution, and final fate, up to 4 weeks post-transplantation. Moreover, by comparing the obtained *in vivo* CT values (gold volume and density) to the actual number of GNP-loaded MSCs in each brain region (measured *ex vivo* by atomic absorption technique), we established a CT quantitative ruler that can extrapolate the exact number of cells within each brain region in a nondestructive manner.

Another novel aspect of this work was the application of our cell tracking technique in a rat model for depression. This common and disabling neuropsychiatric condition is associated with significant morbidity and a lifetime prevalence approaching 17%.²⁶ Despite substantial advancement in psychopharmacology and psychotherapy over the last decades,²⁷ current available therapies treat symptoms only, and are far from ideal, with delayed onset and response rates hovering at approximately 65%, and even worse full remission rates.²⁸ Thus, there is a genuine need for the development and improvement of new treatments. Accordingly, we recently examined MSC transplantation as a novel therapeutic for depression.²⁹ We revealed that intracerebroventricular transplantation of MSCs in the Flinders Sensitive Line (FSL), a rat model for depression,³⁰ caused significant improvement in behavioral parameters, and increased neurogenesis in the ipsilateral dentate gyrus and hippocampus²⁹ of FSL rats.

Further development of longitudinal *in vivo* cell tracking abilities, along with behavioral measurements, is fundamental for elucidating the specific biological activity of transplanted MSCs, and for optimizing treatment strategies,³¹ in particular those for cell therapy of neuropsychiatric disorders. Therefore, in the present study, we utilized our long-term and noninvasive cell tracking technique to trace migration and final engraftment location of GNP-loaded MSCs in the FSL rat brain, over one month. The implanted cells were imaged and traced using a CT imaging technique, while the behavioral effects of our novel cell therapy technique were concurrently assessed.

RESULTS AND DISCUSSION

First, we ran *In vitro* experiments; in order to provide visibility to the implanted MSCs by CT, we loaded the cells with 20 nm GNPs,³² and examined labeling efficacy *in vitro*.

Synthesis and Characterization of the GNPs. On the basis of a well-established procedure,^{33–35} GNPs were synthesized and then coated with glucose, due to its stability and high cell-uptake rate. The particles were characterized using transmission electron microscopy (TEM), zeta potential measurements, dynamic light scattering (DLS) and UV–vis spectroscopy (Figure 1).

Labeling MSCs with GNPs. A total of 10^6 MSCs from human adipose tissue origin (ADS1-hMSCs) were incubated with GNPs (30 $\mu\text{g}/\text{mL}$) for 3 h. During this period, the gold nanostructures undergo endocytosis, one of the major pathways for cellular uptake of NPs,^{36,37} through a receptor-mediated endocytosis (RME)³⁸ internalization mechanism. We found that the cells were efficiently labeled, as demonstrated in Figures 2a–c. The average amount of gold nanoparticle uptake, analyzed using Flame Atomic Absorption Spectroscopy (FAAS, SpectrAA 140, Agilent Technologies), was 1.1 million (std: 0.12) per cell. The effect of GNP loading on viability, metabolism and proliferation of MSCs was assessed at several time points over an eight-day period, using an MTT cell proliferation assay (Roche Applied Science).³⁹ Differentiation of MSCs was not altered after labeling with GNPs (Figure 3a). Additionally, cell viability was not reduced as compared to control cells without GNPs, throughout the eight-day experiment (Figure 3b).

For the *In vivo* experiments, the FSL rat model for depression was used as a tool to examine the efficacy of our GNP-based imaging technique for long-term cell tracking and imaging within the brain, and to investigate the therapeutic impact of the hMSCs.

Animal Model. FSL rats are a genetic model for depression, exhibiting behavioral and pharmacological features similar to those observed in depressed individuals, such as sleep and immune abnormalities, reduced appetite, anhedonia and reduced psychomotor function, along with neurochemical alterations in the limbic system. Antidepressant treatment of FSL rats has a beneficial effect on the two major symptoms of depression, namely, loss of motivation and anhedonia. Thus, the FSL model is useful for screening treatments for depression in a controlled paradigm.^{40,31–39,30}

***In Vivo* Experimental Design.** FSL rats ($n = 23$), and control Sprague–Dawley (SD) rats ($n = 9$) were habituated to the animal housing room, then baseline behavioral measurements of immobility were conducted using the forced swim test (FST). This well-established test indicates levels of despair and motivation, interpreted as depressive-like behavior.³⁰ All rats then underwent stereotaxic surgery, in which a syringe

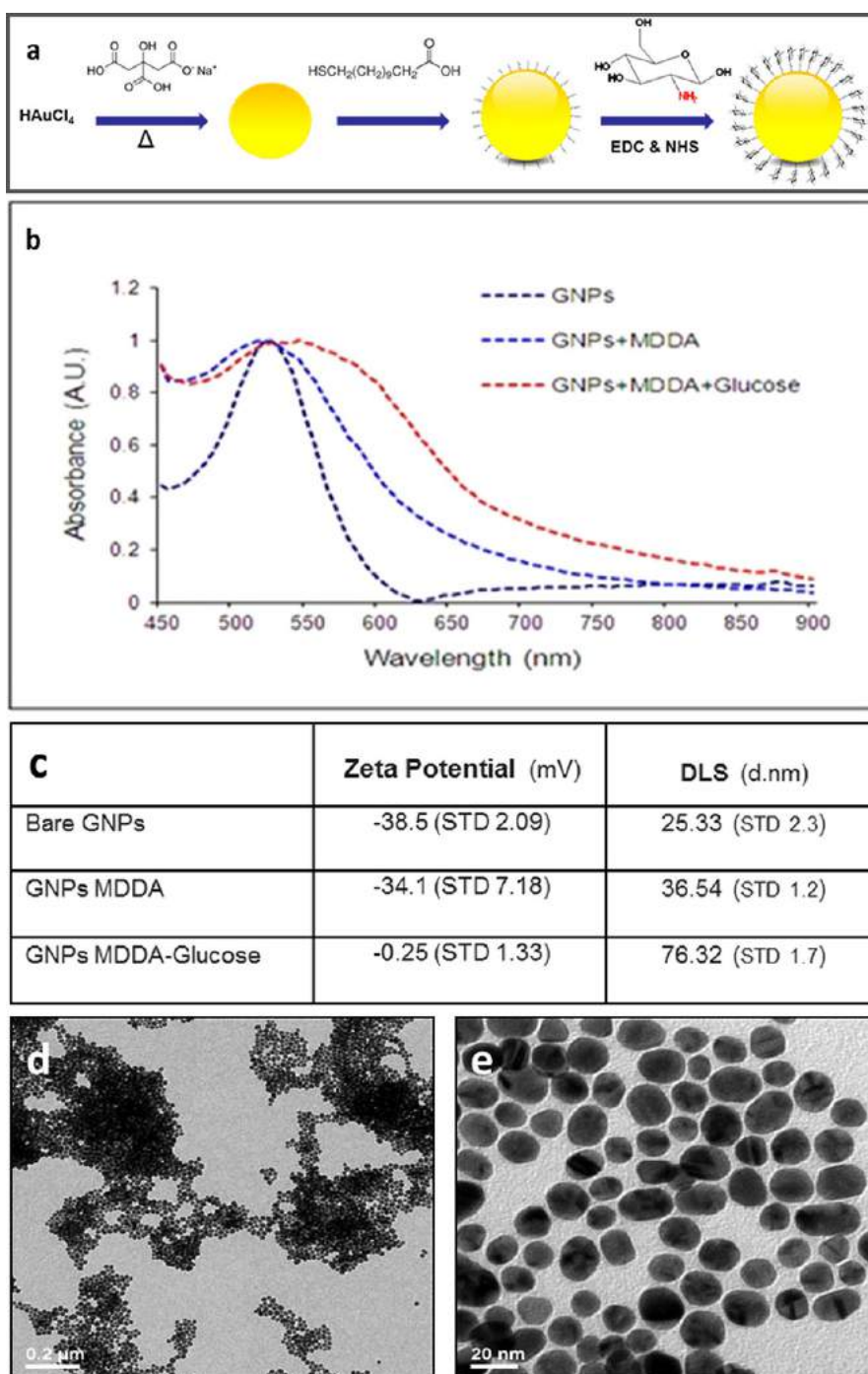


Figure 1. Characterization of GNPs. (a) Schematic diagram of the GNPs synthesis process: the GNPs were conjugated to the linker MDDA (12-mercaptododecanoic acid, Sigma) followed by covalent conjugation to glucose (GLU) (*D*-(+)-glucosamine hydrochloride, Sigma-Aldrich, Israel Ltd.). (b) Optical properties of GNPs: ultraviolet–visible spectroscopy of bare GNPs, MDDA coated GNPs, and glucose-MDDA coated GNPs. (c) Zeta potential measurements (at 25 °C) at the various stages of GNP coatings and dynamic light scattering size measurements. The significant difference that was obtained (by zeta potential, DLS and UV–vis spectroscopy) following each chemical step demonstrates the efficiency of the chemical coating. It should be noted that the zeta potential of the GF-GNP was near zero, due to full coverage of the NP surface. (d) Transmission electron microscopy image of 20 nm GNPs (scale bar 20 nm).

was inserted into the left lateral ventricle (coordinates: anterior -0.8 , lateral 1.5 , ventral -4.0 mm from the bregma). For injection of cells or vehicle through the syringe, rats were divided into seven groups: (1) FSL rats ($n = 6$) treated with 2×10^5 ADS1-hMSCs (total volume $10 \mu\text{L}$), (2) FSL rats ($n = 3$) treated with 2×10^5

ADS1-hMSCs loaded with GNPs (total volume $10 \mu\text{L}$), (3) control FSL rats ($n = 6$) that received saline only ($10 \mu\text{L}$), (4) control FSL rats ($n = 2$) that received free GNPs (saline with GNPs; $10 \mu\text{L}$; 30 mg/mL), (5) control SD rats ($n = 2$) treated with 2×10^5 ADS1-hMSCs loaded with GNPs (total volume $10 \mu\text{L}$), (6) naïve control SD rats

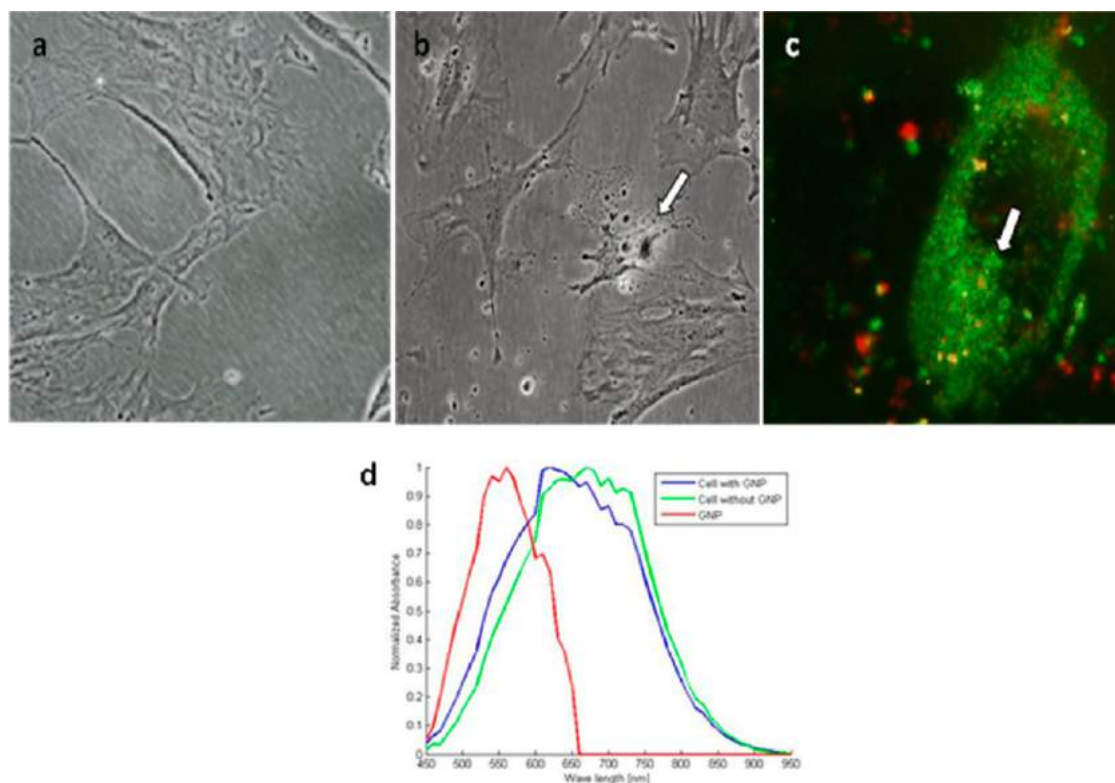


Figure 2. MSCs labeled with GNPs: (a) bright field microscopy of hMSCs without GNPs; (b) bright field microscopy of hMSCs uploaded with GNPs; (c) dark field microscopy of one hMSC (green) uploaded with GNPs (yellow-red); (d) normalized reflectance spectra of hMSCs uploaded with GNPs (blue), hMSCs without GNPs (green), and the uploaded GNPs (red). The spectrum of the GNPs (red) was obtained after reduction of the background signal (hMSCs without GNPs) from the total reflectance signal (hMSCs with GNPs), to emphasize the presence of uploaded GNPs.

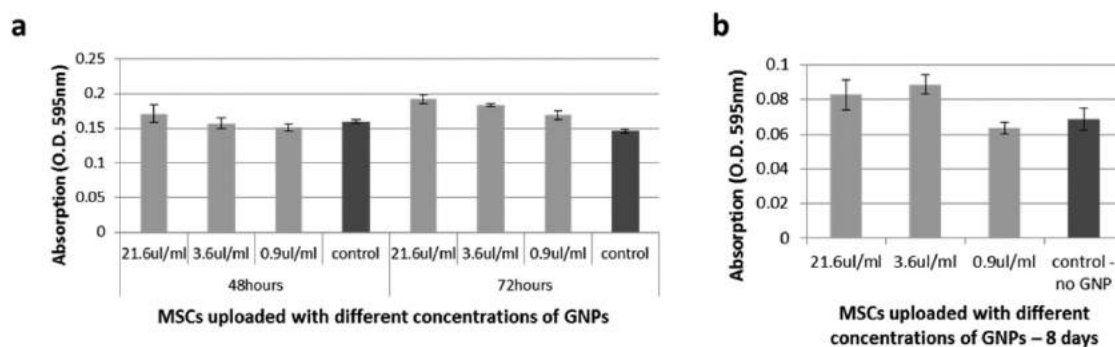


Figure 3. MTT cells proliferation assay: (a) short-term (48 and 72 h). (b) long-term (8 days). Proliferation of the MSCs remained unaltered following labeling with GNPs. In addition, cell viability was not reduced as compared with control cells without GNPs, up to 8 days after labeling. The absorbance readings (OD) of the MSCs were taken at 595 nm. Values presented as mean \pm SD.

($n = 7$) and (7) naïve FSL rats ($n = 6$). On days 14–20, depressive-like behavior in the sucrose consumption test was examined. On day 21, depressive-like behavior in the forced swim test was examined again in all groups. These two tests are a measure for the two core symptoms that identify major depression, *i.e.*, loss of motivation (represented by the forced swim test)^{30,41} and anhedonia (represented by the sucrose consumption test).⁴² During the experiment, animals that received either hMSCs loaded with GNPs or GNPs alone

were CT scanned at several time points (Figure 4). Following *in vivo* investigations, brains were removed for further *ex vivo* scans, and gold volume and location analysis. In addition, brains from several rats in each experimental group were removed for further immunohistochemical analysis. The *in vivo* research timeline is shown in Figure 4.

In Vivo CT Imaging. For tracking the migration and exact localization of GNP-labeled hMSCs, we conducted *in vivo* CT scans at several time points

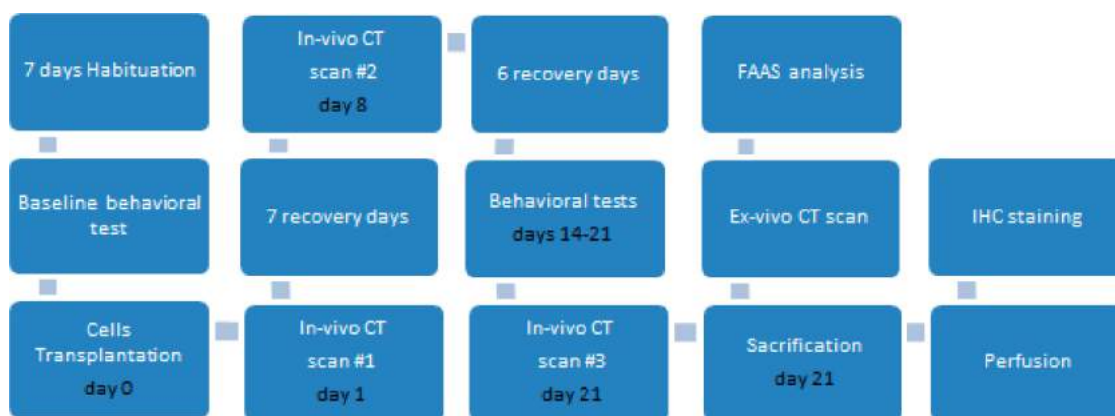


Figure 4. *In vivo* research timeline.

post-transplantation (up to 4 weeks). Images were obtained using a micro-CT device (Skyscan 1176, Bruker micro-CT, Kontich, Belgium), and the projection images were reconstructed into cross-sectional slices (NRecon v.1.6.9, Bruker micro-CT). Figure 5 displays 3D images obtained 1 h (Figure 5a), 1 day (Figure 5b), and one month post GNP-labeled hMSCs injection (Figure 5c), and as a control, one month post GNP injection (Figure 5d). As demonstrated, cell migration could be detected as early as 24 h post-transplantation: the cells which were implanted at a specific location within the left ventricle, were found in a much wider area 1 day later (Figure 5b). Additionally, we observed a notable difference between spatial distributions of the injected GNP-labeled hMSCs and the free GNPs (control group). After one month, free GNPs (Figure 5d) were scattered and widely spread within the brain, symmetrically in both hemispheres, while the GNP-labeled hMSCs appear to have concentrated in specific regions (Figure 5c). We could also trace migration of cells over time in each specific coronal brain slice. Figure 5e–g demonstrate a representative coronal brain slice, which shows a clear difference between cell location 1 week post-transplantation (Figure 5e) and 3 weeks post-transplantation (Figure 5f). The actual direction of migration within this coronal slice is visualized in Figure 5g, displaying both scans together.

We further verified the migration pattern of the hMSCs by calculating both the gold volume in the brain (# of voxels containing gold) and the average density within these voxels, over time. We found (Figure 5h,i) that the volume of the GNP-labeled hMSCs decreased (from 20 000 to 7500 voxels), while average density increased (from 93CT# to 138CT#), verifying the homing of the hMSCs over the experimental period. In contrast, an opposite trend was observed for the control group injected with free GNPs. The volume of the GNPs increased (from 19 800 to 25 483 voxels), while average density decreased (from 94CT# to 90CT#), showing nonspecific distribution of the GNPs. The different distribution patterns of GNP-loaded hMSCs and free GNPs

could also denote that the GNPs remained within the hMSCs throughout the experiment.

In addition, to validate the specificity of the above migration pattern, we ran the same scans and analyses on the control SD rats. Figure 7a,b demonstrates a different MSC migration pattern of the control SD rats. The GNPs did not accumulate in a specific area, but rather diffused and scattered into many regions, in such a way that after one month, the gold was almost undetectable. The total detectable gold volume was only 347 voxels, and its density was 119, which are both lower than those in treated FSL rats. These *in vivo* CT results (Figures 5 and 7) unequivocally show that the MSCs in the FSL rat were specifically navigated and homed to regions that may be correlated with depression.

Ex Vivo CT Imaging. One month post injection, we further examined the exact location, distribution and final fate of the hMSCs *ex vivo*, using contrast agents, and higher resolution and radiation dose. Figure 6a shows a representative image of a coronal *ex vivo* CT section of rat brain one month post GNP-loaded hMSC injection, and a corresponding rat brain atlas reference. It is clearly demonstrated that the hMSCs accumulated into specific areas in the left hemisphere, mostly in the cingulate cortex (Figure 6a), an area recently linked to depression.^{43,44} In contrast, control FSL GNPs remained at the injection site (Figure 6b). The *ex vivo* scans of control SD rats indicated that the only location in which a small amount of gold was still detectable after one month was at the left ventricle (Figure 7c).

Cell Quantification. To quantify the exact amount of cells that reached each brain region, tissues from 30 different brain regions were excised and analyzed using FAAS. Figure 6c,d demonstrates the different brain regions and the exact number of engrafted cells in each region. The different migration patterns between hMSCs and free GNPs are clearly notable: while for FSL controls GNPs are detected in many different regions on both hemispheres and mostly in the ventricles, in treated rats the hMSCs can be found mainly in

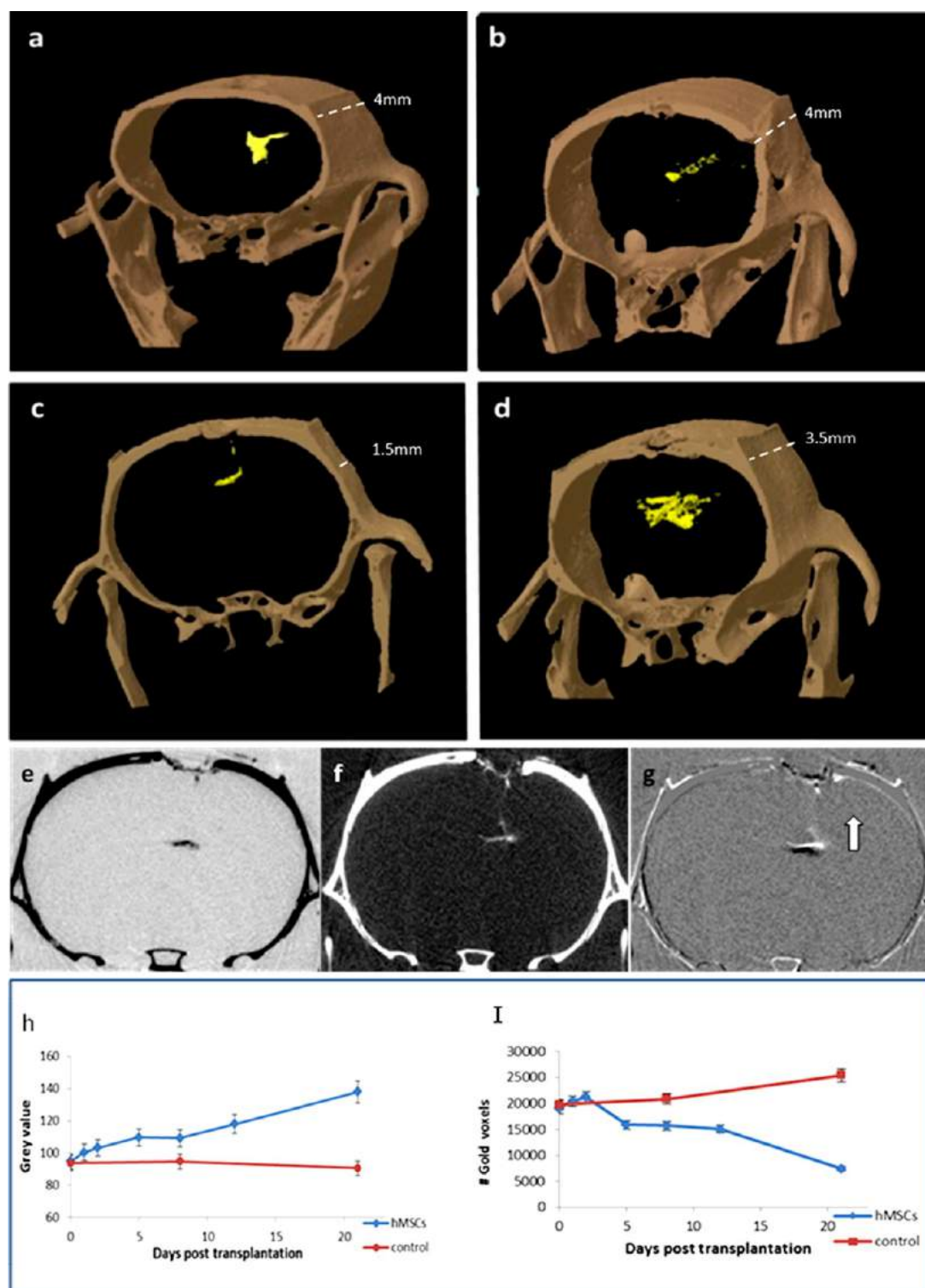


Figure 5. (a–d) 3D *in vivo* volume rendering micro-CT scans of brains post GNP-labeled hMSC injection into the left ventricle: (a) 1 h post injection; (b) 24 h post injection; (c) one month post injection; (d) one month post free GNP injection (control rat). (e–g) Longitudinal migration tracking changes: (e) coronal brain slice 1 week post-transplantation (GNPs appear black), (f) the same coronal brain slice 3 weeks post-transplantation (GNPs appear white); (g) displays actual migration within this coronal slice by overlapping the two scans (arrow indicates migration direction). CT scans were obtained using CT Data Viewer registration application. (h) Longitudinal measurements of average CT density (gray values) of the injected hMSCs and the injected free GNPs (control). (i) longitudinal measurements of the number of voxels containing gold, post hMSC injection or free GNP injection (control).

the cingulate cortex (approximately 85 000 cells). Cell quantification for the control SD rats revealed small

amounts of cells that diffused into many brain regions (Figure 7d).

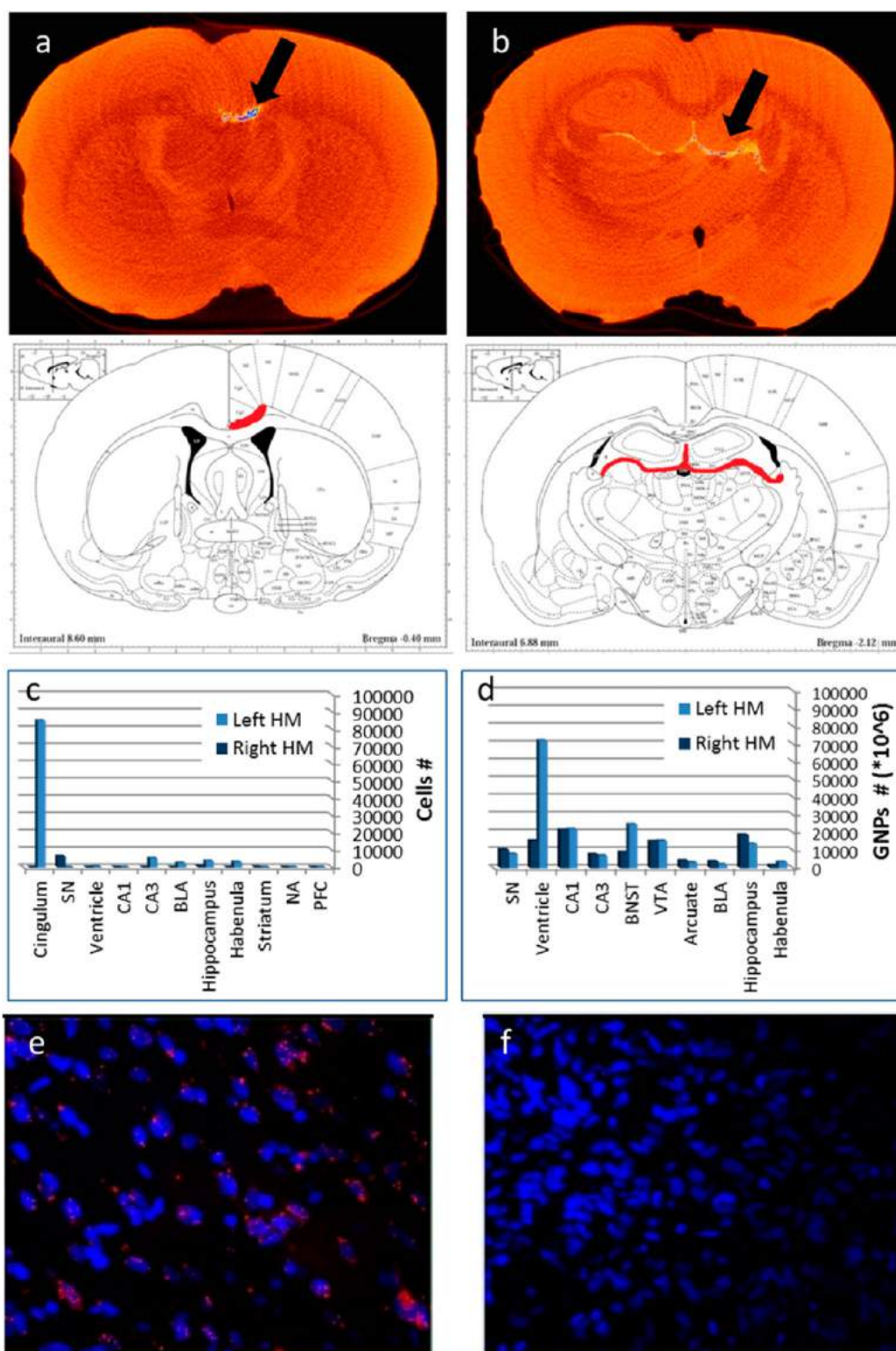


Figure 6. Localization of mesenchymal stem cells in the brain one month post-transplantation. Top panels: (a) representative *ex vivo* coronal CT images, obtained one month post hMSC transplantation, and (b) one month post GNP injection; bottom panels: (a and b) corresponding reference to relevant brain sections from rat brain atlas (Paxinos and Watson). Images used with permission from ref 53. Copyright Elsevier 2006. (c and d) FAAS analysis of 16 bihemispheric punches ((c) hMSCs; (d) control). Abbreviations: SN, substantia nigra; BLA, basolateral amygdala; CA, central amygdala; NA, nucleus accumbens; PFC, prefrontal cortex; BNST, bed nucleus of stria terminalis; VTA, ventral tegmental area. (e and f) Immunohistochemical analysis; representative coronal brain slices corresponding to regions with the majority of detected gold (c and d), stained with mouse anti-human mitochondria monoclonal primary antibody (Millipore MAB1273, 1:400), and subsequently visualized with an Alexa Fluor 568 goat anti-mouse secondary antibody (1:1000, red) as well as DAPI staining (blue). Fluorescent images were acquired using an Olympus confocal microscope ($\times 60$) ((e) hMSCs; (f) control).

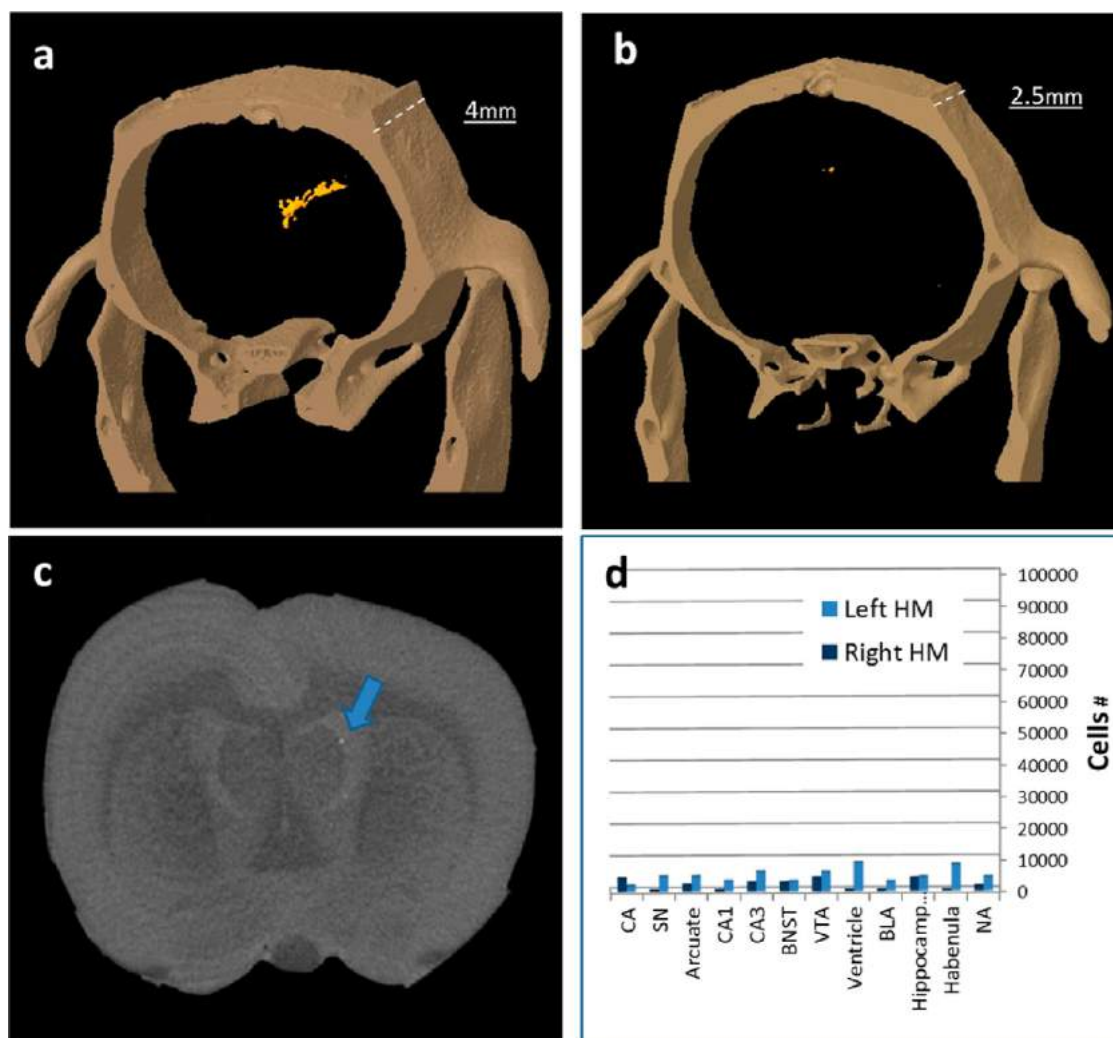


Figure 7. Migration and localization of mesenchymal stem cells in control SD rat brain. Top panels: 3D *in vivo* volume rendering micro-CT scans of brains post GNP-labeled hMSC injection; (a) 1 day post injection; (b) one month post injection. Bottom panels: Localization of mesenchymal stem cells in the brain one month post-transplantation; (c) representative *ex vivo* coronal CT image, obtained one month post hMSC transplantation; (d) FAAS analysis of 16 bihemispheric punches. Abbreviations: SN, substantia nigra; BLA, basolateral amygdala; CA, central amygdala; NA, nucleus accumbens; BNST, bed nucleus of stria terminalis; VTA, ventral tegmental area.

CT Quantitative Ruler. Next, to quantify the exact number of migrated hMSCs using nondestructive means, we developed a noninvasive quantitative CT ruler. This ruler was established by comparing the obtained *in vivo* CT values (gold volume and density) to the actual number of the GNP-loaded hMSCs in each brain region, measured by *ex vivo* atomic absorption technique. In this method, we determined the number of cells per voxel (C/V) by dividing the total number of injected cells by the number of gold voxels immediately post-transplantation (in our experiment: 250 000 cells/19 094 voxels = ~ 13 cell/voxel). By multiplying the calculated C/V value by the differential density (ρ) and the number of gold voxels (V) in each region of interest, we were able to determine the number of cells in each region. To confirm the validity of this quantitative CT ruler, we compared the number of cells calculated in this method to the actual

number measured by the *ex vivo* atomic absorption technique.

We used this quantitative CT ruler to calculate the number of cells that reached the cingulate cortex one month post-transplantation. The differential density within this area was $\rho = 1.46$ (average gray value post-transplantation divided by the average gray value pretransplantation: $\rho = 138/94 = 1.46$), and the number of gold voxels within this area was $V = 4500$. Thus, the estimated number of cells in the cingulate cortex was: $C/V \times \rho \times V = 13 \times 1.46 \times 4500 = 85\,410$. This result matches the actual number of cells that reached this area (84 923 cells), quantified using *ex vivo* FAAS (dividing actual gold amount with average number of particles loaded in each cell [$\sim 1 \times 10^6$; the amount uploaded in the *in vitro* experiments]). Thus, we demonstrate that our quantitative CT ruler can be used to determine the number of cells residing in a specific

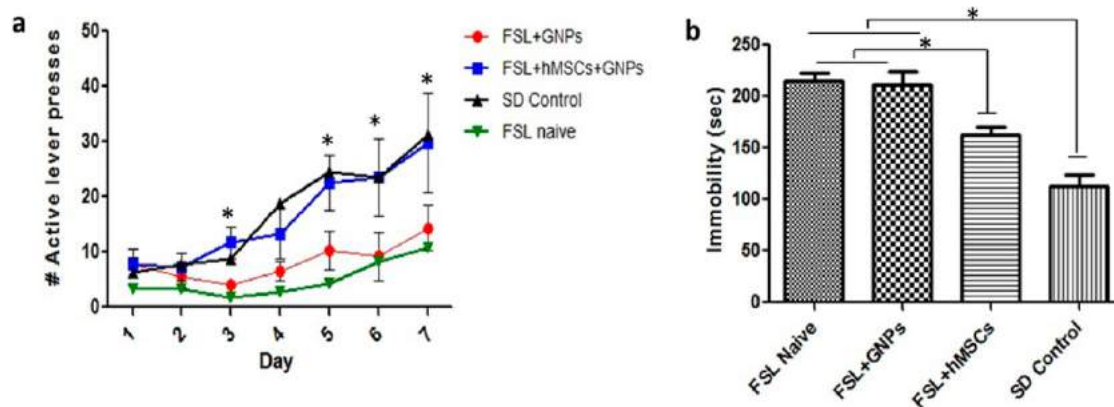


Figure 8. Effect of MSC transplantation on depressive-like behavior: (a) sucrose consumption test, 2 weeks post-transplantation, displaying active lever presses over 7 consecutive days in rats treated with hMSCs and in naïve SD, naïve FSL, and FSL with GNPs as control groups. Treated rats showed a significantly higher number of active lever presses as compared with the nontreated FSL rats ($p < 0.05$). (b) Forced swim test scores, 21 days post-transplantation, for rats that received hMSCs treatment and for naïve SD, naïve FSL, and FSL with GNPs only as control groups. Treated rats showed significantly reduced immobility time ($p < 0.05$).

brain region, without tissue destruction or animal sacrifice.

Immunohistochemistry. To confirm the CT and FAAS results, which located MSCs based on their uploaded gold particles, we performed immunohistochemical staining, which locates the cells based on antibody labeling (Figure 6e,f). Using this method, the injected MSCs from human origin can easily be distinguished from rat cells. As shown in Figure 6a,b, the MSCs are indeed present in the slices taken from regions found to contain GNPs (in the *ex vivo* CT), one month post-transplantation.

Behavioral Results. To evaluate the therapeutic effect of the cell-based treatment on depressive-like behavior, we performed tests that measure core symptoms of depression, *i.e.*, the sucrose consumption test,⁴⁵ which assesses anhedonia, followed by the forced swim test,⁴¹ which measures loss of motivation. The sucrose consumption test was performed on days 14–20 post-transplantation, in FSL rats which received hMSCs treatment, and in three control groups (naïve SD, naïve FSL and FSL treated with GNPs only). Figure 8a displays active lever presses during the 7 consecutive days of the experiment. Repeated measures ANOVA for active lever presses revealed a main effect of group [$F(3,144) = 4.71$; $p < 0.01$], main effect of days [$F(6,144) = 16.58$; $p < 0.0001$] and main effect of interaction (groups \times days) [$F(18,144) = 1.93$; $p < 0.01$]. The hMSC-treated FSL rats showed a significantly higher number of active lever presses as compared with nontreated FSL rats, similar to the SD control group (Bonferroni's multiple comparison post-hoc test ($p < 0.05$)). Figure 8b displays the Forced Swim test results 21 days post-transplantation. A significant difference in immobility time was observed comparing hMSC-injected FSL rats with the naïve FSL control group, or with GNP-injected FSL rats (one way ANOVA and

Bonferroni's multiple comparison post-hoc test, $p < 0.05$). The hMSC-treated group showed attenuated depressive-like behavior, narrowing the difference between the FSL group behavior and the control SD group. This indicates that hMSC treatment effectively attenuated depressive-like behavior. In addition, rats injected with GNP-loaded MSCs showed the same behavioral patterns as those injected with MSCs only, indicating that the GNPs are nontoxic and do not affect hMSCs migration properties or any other biological activity.

CONCLUSIONS

In conclusion, this work demonstrates a novel, noninvasive imaging technique for labeling and real-time, prolonged tracking of stem cells. These key features, which pose a challenge particularly within deep brain structures that are difficult to access, or even completely inaccessible,^{46,47} have the potential to elucidate poorly understood mechanisms underlying the success or failure of cell therapy. Our research further reveals that cell therapy is a beneficial approach for treating neuropsychiatric disorders. Behavioral manifestations of the two core symptoms of depressive behavior, *i.e.*, lack of motivation and anhedonia, were both significantly attenuated following treatment, indicating the efficacy of an MSC-based therapy approach. We found that the cells were engrafted mainly in the cingulate cortex, which has been recently linked to neuropsychiatric conditions.^{43,44} Recent clinical studies in patients with Major Depression Disorder (MDD) found that depression severity correlates with reduced white matter integrity in several prefrontal areas, including the anterior cingulum.^{48–50} Future research utilizing the suggested technique can provide quantitative information regarding the effect of MSCs on depressive

behavior, concurrently with elucidation of the mechanisms underlying the beneficial effect of these cells. We expect this novel CT-based cell tracking

technique to lead to a significant improvement in cellular therapy both for basic research and novel therapeutic approaches.

METHODS

GNP Synthesis. *Synthesis.* A total of 0.414 mL of 1.4 M HAuCl_4 solution in 200 mL of water was added to a 250 mL single-neck round-bottom flask and the solution was stirred in an oil bath on a hot plate until it boiled. Then, 4.04 mL of a 10% sodium citrate solution (0.39 M sodium citrate tribasic dihydrate 98%, Sigma CAS 6132-04-3) was quickly added. The solution was stirred for 5 min, and then the flask was removed from the hot oil and placed aside until it cooled.

Conjugation. To prevent aggregation and stabilize the particles in physiological solutions, MDDA (96%, Sigma-Aldrich, Israel Ltd.) was adsorbed onto the GNPs. This layer also provides the chemical groups required for antibody conjugation ($-\text{COOH}$). First, the solution was centrifuged to dispose of excess citrate. MDDA solution (2.26×10^{-3} g) was then added to the GNP solution, and the mixture was stirred overnight and placed in a centrifuge in order to dispose of excess MDDA. Next, excess EDC (*N*-ethyl-*N*-(3-(dimethylamino)propyl)carbodiimide) (1.87×10^{-3} g) and NHS (*N*-hydroxysuccinimide) (Thermo Fisher Scientific, Inc., Rockford, IL) (2.12×10^{-3} g) were added to the solution, followed by addition of glucose-2 (2GF) ($\text{D}(+)\text{-glucosamine hydrochloride}$, Sigma-Aldrich, Israel Ltd.) (1.75×10^{-3} g). NHS and EDC form an active ester intermediate with the $-\text{COOH}$ functional groups, which can then undergo an amidation reaction with the glucose $-\text{NH}_2$ group. Glucosamine molecule C-2 (2GF-GNP): $\text{D}(+)\text{-glucosamine hydrochloride}$ (3 mg; Sigma-Aldrich) was added to the activated linker-coated GNPs.

Human-MSCs ADS1 (hMSCs) Isolation and Expansion. hMSCs were isolated from adult human subcutaneous adipose tissue, as previously described.⁴⁶ The cells were plated in T-225 tissue culture flasks (Corning, Corning, NY) and cultured with mesenchymal stem cell growth medium and preadipocyte growth medium (Cambrex Bio Science), respectively, at 37 °C in 5% CO_2 and 90% humidity. The medium was changed every 3 days.

Cell Uploading with GNP. MSC cells (2.5×10^6) were cultured in 5 mL of glucose-free DMEM medium containing 5% FCS, 0.5% penicillin, and 0.5% glutamine. GNPs were then added in excess (one million particles per cell). The cells were then incubated at 37 °C for 3 h. After incubation, the medium was washed twice with PBS, followed by trypsin treatment; the cells were centrifuged twice (7 min in 1000 rpm) to wash out unbound nanoparticles.

Animal Care. All animals were maintained on a 12:12 h light/dark cycle under fixed conditions of temperature (23 °C) and humidity (50%), with free access to food and water. Rats were habituated to the animal housing room for 7 days before conducting the experimental procedures. All experimental procedures were approved by the Animal Care Committee of Bar-Ilan University and in accordance with the NIH Guide for the Care and Use of Laboratory Animals.

MSC Implantation. Animals were anesthetized with ketamine hydrochloride (100 mg/kg, ip) and xylazine (10 mg/kg, ip), then placed in a David Kopf stereotaxic apparatus. A hole was drilled through the skull and a 10 μL Hamilton syringe was lowered unilaterally into the lateral ventricles (anterior -0.8 , lateral 1.5, ventral -4.0 mm from the bregma). GNP-loaded hMSCs or hMSCs alone ($\sim 2 \times 10^5$, 10 μL), vehicle + GNPs (10 μL , 30 mg/mL), or saline (10 μL) was infused through the syringe over 5 min, at 2 $\mu\text{L}/\text{min}$. Upon completion of the surgeries, antibiotics (Baytril, 0.4 mL, s.c.) and analgesics (Rimadyl, 0.05 mL, s.c.) were administered for 3 consecutive days.

In Vivo Micro-CT Scans. *In vivo* scans of rats were performed with nominal resolution (pixel size) of 36 μm , employing an aluminum filter 0.5 mm thick and an applied X-ray tube voltage of 45 kV, in order to obtain a shorter radiation time and lower radiation dose for the live rat. Surface-rendered 3D models were

constructed for 3D viewing of the analyzed brain regions. Volume rendered 3D images were generated using an RGBA transfer function in SkyScan CT-Volume ("CTVol") software.

Ex Vivo Micro-CT Scans. For the *ex vivo* scans, we used an additional contrast agent, because there is very little difference in density and X-ray absorption over different brain tissue types, *i.e.*, no native CT contrast. We used a procedure based on studies by Crespigny¹⁹ and Saito,⁴⁷ and modified by us to apply to rat brains, using a nonionic iodinated contrast agent (Iopamidol, Bayer Schering Pahrma, Japan). Brains were removed and placed in 10% buffered formalin for 5 days of fixation, then soaked in Iopamidol (150 mg/mL) diluted with 7.5% paraformaldehyde, at 4 °C for 14 days. Prior to CT imaging, brains were removed from the solution, blotted dry and placed in a sample holder for imaging. The sample holder was sealed with plastic film to prevent dehydration. Brains were then scanned in the micro-CT at a nominal resolution (pixel size) of 9 μm , employing an aluminum filter 0.2 mm thick and an applied X-ray tube voltage of 45 kV. Camera pixel binning of 2×2 was applied. The scan orbit was 180 with a rotation step of 0.4°. Reconstruction was carried out with a modified Feldkamp⁵¹ algorithm using the SkyScan NRecon software accelerated by GPU.⁵² Gaussian smoothing (2%), ring artifact reduction and beam hardening correction (20%) were applied. The cross-section slices were stored in 8-bit BMP format (256 shades of gray).

Flame Gold Analysis. The tissues obtained from the experimental animals were melted with *aqua regia* acid, a mixture of nitric acid and hydrochloric acid in a volume ratio of 1:3. The samples were then evaporated, filtered and diluted to a final volume of 5 mL. Au lamp was used in order to determine the gold concentration in the samples. A calibration curve with known gold concentrations was prepared (commonly: 0.1, 1, 2 and, 5 mg/mL). Gold concentration in each sample was determined according to its absorbance value with correlation to the calibration curve. Each sample was analyzed in triplicate and averages and standard deviations were taken.

Immunohistochemistry. Animals were sacrificed 21 d post-surgery, under deep anesthesia, by transcardial perfusion with PBS $\times 1$ followed by 4% paraformaldehyde. Excised brains were post-fixed in paraformaldehyde for 48 h at 4 °C, then equilibrated in PBS containing 30% sucrose for an additional 48 h at 4 °C. Fixed brains were gradually frozen in dry ice and stored at -80 °C until use. Tissues were cryosectioned at 30 μm in the coronal plane, then immersed in 0.02% sodium azide and washed in PBS. Sections were then blocked with a blocking solution and stained with anti-human mitochondria monoclonal primary antibody (Millipore MAB1273, 1:400) and subsequently visualized with an Alexa Fluor 568 goat anti-mouse secondary antibody (1:1000, red) as well as DAPI staining (blue). Fluorescent images were acquired using an Olympus confocal microscope ($\times 60$).

Forced Swim Test. To examine depressive-like behavior in rats, the forced swim test⁴¹ was performed (21 days post cells transplantation). Rats were placed in a cylindrical tank (height, 40 cm; diameter, 18 cm) containing just enough water (at 2 °C above room temperature) so that the rat could not touch the bottom with its hind paws. The amount of time that each rat either swam or stayed immobile during a 5 min period was recorded. Immobility was defined as suspension of swimming, in such a manner that both hind paws were immobile, indicating depressive behavior (despair, or lack of motivation). Behavior in the forced swim test was measured using Noldus Ethovision 7.0 XT.

Sucrose Consumption Test. To examine depressive-like behavior in rats, the sucrose self-administration test was used. Rats were transferred into operant conditioning chambers (Med-Associates, Inc.; St Albans, VT) for daily 30 min sessions, during

their dark cycle. Each self-administration chamber (30 cm × 25 cm × 22 cm) had two levers, active and inactive, located 5 cm above the floor of the chamber. An active lever press delivered sucrose (20% sucrose solution; 0.13 mL/infusion; duration of 5 s) through an infusion pump and into a liquid drop receptacle for oral consumption. A light located above the active lever was lit during the 5 s-long sucrose infusion periods, and remained lit for another 15 s. Throughout these 15-s intervals, active lever presses were recorded, but no additional sucrose reinforcement was provided. Presses on the inactive lever were recorded, but they did not activate the infusion pump and light. Rats were returned to their home cages at the end of the daily session. The test was performed daily, for 7 consecutive days (14–20 days post cells transplantation).

Conflict of Interest: The authors declare no competing financial interest.

REFERENCES AND NOTES

- Chang, J.-W.; Hung, S.-P.; Wu, H.-H.; Wu, W.-M.; Yang, A.-H.; Tsai, H.-L.; Yang, L.-Y.; Lee, O. K. Therapeutic Effects of Umbilical Cord Blood-Derived Mesenchymal Stem Cell Transplantation in Experimental Lupus Nephritis. *Cell Transplant.* **2011**, *20*, 245–257.
- Ra, J. C.; Shin, I. S.; Kim, S. H.; Kang, S. K.; Kang, B. C.; Lee, H. Y.; Kim, Y. J.; Jo, J. Y.; Yoon, E. J.; Choi, H. J.; *et al.* Safety of Intravenous Infusion of Human Adipose Tissue-Derived Mesenchymal Stem Cells in Animals and Humans. *Stem Cells Dev.* **2011**, *20*, 1297–1308.
- Sensebé, L.; Tarte, K.; Galipeau, J.; Krampera, M.; Martin, I.; Phinney, D. G.; Shi, Y. Limited Acquisition of Chromosomal Aberrations in Human Adult Mesenchymal Stromal Cells. *Cell Stem Cell* **2012**, *10*, 9–10; author reply 10–11.
- Uccelli, A.; Laroni, A.; Freedman, M. S. Mesenchymal Stem Cells for the Treatment of Multiple Sclerosis and Other Neurological Diseases. *Lancet Neurol.* **2011**, *10*, 649–656.
- Bone, H.; Stromal, M. M.; Expressing, C.; Vehicle, C. D.; Therapy, H. G. Human Bone Marrow-Derived Mesenchymal Stromal Cells. *Stem Cells* **2009**, 2320–2330.
- Meirelles, L. D. S.; Fontes, A. M.; Covas, D. T.; Caplan, A. I. Mechanisms Involved in the Therapeutic Properties of Mesenchymal Stem Cells. *Cytokine Growth Factor Rev.* **2009**, *20*, 419–427.
- Joyce, N.; Annett, G.; Wirthlin, L.; Olson, S.; Bauer, G.; Nolte, J. a. Mesenchymal Stem Cells for the Treatment of Neurodegenerative Disease. *Regen. Med.* **2010**, *5*, 933–946.
- Crigler, L.; Robey, R. C.; Asawachaicharn, A.; Gaupp, D.; Phinney, D. G. Human Mesenchymal Stem Cell Subpopulations Express a Variety of Neuro-Regulatory Molecules and Promote Neuronal Cell Survival and Neurogenesis. *Exp. Neurol.* **2006**, *198*, 54–64.
- Ricles, L. M.; Nam, S. Y.; Sokolov, K.; Emelianov, S. Y.; Suggs, L. J. Function of Mesenchymal Stem Cells Following Loading of Gold Nanotracers. *Int. J. Nanomed.* **2011**, *6*, 407–416.
- Karp, J. M.; Leng Teo, G. S.; Mesenchymal Stem, Cell Homing: The Devil Is in the Details. *Cell Stem Cell* **2009**, *4*, 206–216.
- Ankrum, J.; Karp, J. M. Mesenchymal Stem Cell Therapy: Two Steps Forward, One Step Back. *Trends Mol. Med.* **2010**, *16*, 203–209.
- Janowski, M.; Bulte, J. W. M.; Walczak, P. Personalized Nanomedicine Advancements for Stem Cell Tracking. *Adv. Drug Delivery Rev.* **2012**, *64*, 1488–1507.
- Stuckey, D. J.; Carr, C. a.; Martin-Rendon, E.; Tyler, D. J.; Willmott, C.; Cassidy, P. J.; Hale, S. J. M.; Schneider, J. E.; Tatton, L.; Harding, S. E.; *et al.* Iron Particles for Noninvasive Monitoring of Bone Marrow Stromal Cell Engraftment Into, and Isolation of Viable Engrafted Donor Cells From, the Heart. *Stem Cells* **2006**, *24*, 1968–1975.
- Phinney, D. G.; Prockop, D. J. Concise Review: Mesenchymal Stem/Multipotent Stromal Cells: The State of Trans-differentiation and Modes of Tissue Repair—Current Views. *Stem Cells* **2007**, *25*, 2896–2902.
- Shihabuddin, L. S.; Aubert, I. Stem Cell Transplantation for Neurometabolic and Neurodegenerative Diseases. *Neuropharmacology* **2010**, *58*, 845–854.
- Villa, C.; Erratico, S.; Razini, P.; Fiori, F.; Rustichelli, F.; Torrente, Y.; Belicchi, M. Stem Cell Tracking by Nanotechnologies. *Int. J. Mol. Sci.* **2010**, *11*, 1070–1081.
- Xu, C.; Mu, L.; Roes, I.; Miranda-Nieves, D.; Nahrendorf, M.; Ankrum, J. a.; Zhao, W.; Karp, J. M. Nanoparticle-Based Monitoring of Cell Therapy. *Nanotechnology* **2011**, *22*, 494001.
- Frangioni, J. V.; Hajjar, R. J. *In Vivo* Tracking of Stem Cells for Clinical Trials in Cardiovascular Disease. *Circulation* **2004**, *110*, 3378–3383.
- Crespigny, A. de; Bou-Reslan, H. 3D Micro-CT Imaging of the Postmortem Brain. *J. Neurosci. Methods* **2008**, *171*, 207–213.
- Arvizo, R. Gold Nanoparticles: Opportunities and Challenges in Nanomedicine. *Expert Opin. Drug Delivery* **2010**, *7*, 753–763.
- Lasagna-Reeves, C.; Gonzalez-Romero, D.; Barria, M. a.; Olmedo, I.; Clos, a.; Sadagopa Ramanujam, V. M.; Urayama, a.; Vergara, L.; Kogan, M. J.; Soto, C. Bioaccumulation and Toxicity of Gold Nanoparticles after Repeated Administration in Mice. *Biochem. Biophys. Res. Commun.* **2010**, *393*, 649–655.
- Thakor, a S.; Jokerst, J.; Zavaleta, C.; Massoud, T. F.; Gambhir, S. S. Gold Nanoparticles: A Revival in Precious Metal Administration to Patients. *Nano Lett.* **2011**, *11*, 4029–4036.
- El-Sayed, I. H. Nanotechnology in Head and Neck Cancer: The Race Is On. *Curr. Oncol. Rep.* **2010**, *12*, 121–128.
- Zhang, X.-D.; Wu, H.-Y.; Wu, D.; Wang, Y.-Y.; Chang, J.-H.; Zhai, Z.-B.; Meng, A.-M.; Liu, P.-X.; Zhang, L.-A.; Fan, F.-Y. Toxicologic Effects of Gold Nanoparticles *In Vivo* by Different Administration Routes. *Int. J. Nanomed.* **2010**, *5*, 771–781.
- Mieszawska, A. J.; Mulder, W. J. M.; Fayad, Z. A.; Cormode, D. P. Multifunctional Gold Nanoparticles for Diagnosis and Therapy of Disease. *Mol. Pharmacol.* **2013**, *10*, 831–847.
- Kessler, R. C.; Berglund, P.; Demler, O.; Jin, R.; Koretz, D.; Merikangas, K. R.; Rush, a J.; Walters, E. E.; Wang, P. S. The Epidemiology of Major Depressive Disorder: Results from the National Comorbidity Survey Replication (NCS-R). *JAMA J. Am. Med. Assoc.* **2003**, *289*, 3095–3105.
- Berton, O.; Nestler, E. J. New Approaches to Antidepressant Drug Discovery: Beyond Monoamines. *Nat. Rev. Neurosci.* **2006**, *7*, 137–151.
- Machado-Vieira, R. Rapid Onset of Antidepressant Action: A New Paradigm in the Research and Treatment of Major Depression. *J. Clin. Psychiatry* **2008**, *69*, 946–958.
- Tfllin, M.; Sudai, E.; Merenlender, a; Gispán, I.; Yadid, G.; Turgeman, G. Mesenchymal Stem Cells Increase Hippocampal Neurogenesis and Counteract Depressive-like Behavior. *Mol. Psychiatry* **2010**, *15*, 1164–1175.
- Overstreet, D. H.; Wegener, G. The Flinders Sensitive Line Rat Model of Depression—25 Years and Still Producing. *Pharmacol. Rev.* **2013**, *65*, 143–155.
- Aarntzen, E. H. J. G.; Srinivas, M.; Walczak, P.; Janowski, M.; Heerschap, A.; de Vries, I. J. M.; Figdor, C. G.; Bulte, J. W. M.; Oyen, W. J. G. *In Vivo* Tracking Techniques for Cellular Regeneration, Replacement, and Redirection. *J. Nucl. Med.* **2012**, *53*, 1825–1828.
- Popovtzer, R.; Agrawal, A.; Kotov, N. a.; Popovtzer, A.; Balter, J.; Carey, T. E.; Kopelman, R. Targeted Gold Nanoparticles Enable Molecular CT Imaging of Cancer. *Nano Lett.* **2008**, *8*, 4593–4596.
- Enüstün, B. V.; Turkevich, J. Coagulation of Colloidal Gold. *J. Am. Chem. Soc.* **1963**, *85*, 3317–3328.
- Reuveni, T.; Motiei, M.; Romman, Z.; Popovtzer, A.; Popovtzer, R. Targeted Gold Nanoparticles Enable Molecular CT Imaging of Cancer: An *In Vivo* Study. *Int. J. Nanomed.* **2011**, *6*, 2859–2864.
- Aydogan, B.; Li, J.; Rajh, T.; Chaudhary, A.; Chmura, S. J.; Pelizzari, C.; Wietholt, C.; Kurtoglu, M.; Redmond, P. AuNP-DG: Deoxyglucose-Labeled Gold Nanoparticles as X-ray Computed Tomography Contrast Agents for Cancer Imaging. *Mol. Imaging Biol.* **2010**, *12*, 463–467.

36. Chithrani, D. B. Intracellular Uptake, Transport, and Processing of Gold Nanostructures. *Mol. Membr. Biol.* **2010**, *27*, 299–311.
37. Shi Kam, N. W.; Jessop, T. C.; Wender, P. a; Dai, H. Nanotube Molecular Transporters: Internalization of Carbon Nanotube-Protein Conjugates into Mammalian Cells. *J. Am. Chem. Soc.* **2004**, *126*, 6850–6851.
38. Kam, N. W. S.; Liu, Z.; Dai, H. Carbon Nanotubes as Intracellular Transporters for Proteins and DNA: An Investigation of the Uptake Mechanism and Pathway. *Angew. Chem.* **2006**, *118*, 591–595.
39. Petty, R. D.; Sutherland, L. a; Hunter, E. M.; Cree, I. a. Comparison of MTT and ATP-Based Assays for the Measurement of Viable Cell Number. *J. Biolumin. Chemilumin.* **1995**, *10*, 29–34.
40. Zangen, A.; Overstreet, D. H.; Yadid, G. High Serotonin and 5-Hydroxyindoleacetic Acid Levels in Limbic Brain Regions in a Rat Model of Depression; Normalization by Chronic Antidepressant Treatment. *J. Neurochem.* **2002**, *69*, 2477–2483.
41. Slattery, D. a; Cryan, J. F. Using the Rat Forced Swim Test to Assess Antidepressant-like Activity in Rodents. *Nat. Protoc.* **2012**, *7*, 1009–1014.
42. Pucilowski, O.; Overstreet, D. H.; Rezvani, A. H.; Janowsky, D. S. Chronic Mild Stress-Induced Anhedonia: Greater Effect in a Genetic Rat Model of Depression. *Physiol. Behav.* **1993**, *54*, 1215–1220.
43. Greicius, M. D.; Flores, B. H.; Menon, V.; Glover, G. H.; Solvason, H. B.; Kenna, H.; Reiss, A. L.; Schatzberg, A. F. Resting-State Functional Connectivity in Major Depression: Abnormally Increased Contributions from Subgenual Cingulate Cortex and Thalamus. *Biol. Psychiatry* **2007**, *62*, 429–437.
44. Pannekoek, J. N.; van der Werff, S. J. a; van den Bulk, B. G.; van Lang, N. D. J.; Rombouts, S. A. R. B.; van Buchem, M. a; Vermeiren, R. R. J. M.; van der Wee, N. J. A. Reduced Anterior Cingulate Gray Matter Volume in Treatment-Naïve Clinically Depressed Adolescents. *NeuroImage* **2014**, *4*, 336–342.
45. Yadid, G.; Nakash, R.; Deri, I.; Tamar, G.; Kinor, N.; Gispan, I.; Zangen, a. Elucidation of the Neurobiology of Depression: Insights from a Novel Genetic Animal Model. *Prog. Neurobiol.* **2000**, *62*, 353–378.
46. Dicker, A.; Le Blanc, K.; Aström, G.; van Harmelen, V.; Götherström, C.; Blomqvist, L.; Arner, P.; Rydén, M. Functional Studies of Mesenchymal Stem Cells Derived from Adult Human Adipose Tissue. *Exp. Cell Res.* **2005**, *308*, 283–290.
47. Saito, S.; Mori, Y.; Yoshioka, Y.; Murase, K. High-Resolution *ex Vivo* Imaging in Mouse Spinal Cord Using Micro-CT with 11.7T-MRI and Myelin Staining Validation. *Neurosci. Res.* **2012**, *73*, 337–340.
48. Henderson, S. E.; Johnson, A. R.; Vallejo, A. I.; Katz, L.; Wong, E.; Gabbay, V. A Preliminary Study of White Matter in Adolescent Depression: Relationships with Illness Severity, Anhedonia, and Irritability. *Front. Psychiatry* **2013**, *4*, 152.
49. Lyden, H.; Espinoza, R. T.; Pirnia, T.; Clark, K.; Joshi, S. H.; Leaver, a M.; Woods, R. P.; Narr, K. L. Electroconvulsive Therapy Mediates Neuroplasticity of White Matter Microstructure in Major Depression. *Transl. Psychiatry* **2014**, *4*, e380.
50. Zhang, A.; Leow, A.; Ajilore, O.; Lamar, M.; Yang, S.; Joseph, J.; Medina, J.; Zhan, L.; Kumar, A. Quantitative Tract-Specific Measures of Uncinate and Cingulum in Major Depression Using Diffusion Tensor Imaging. *Neuropsychopharmacology* **2012**, *37*, 959–967.
51. Feldkamp, L. A. Practical Cone-Beam Algorithm Sfrdr I _ F. *J. Opt. Soc. Am. A* **1984**, *1*, 612–619.
52. Yan, G.; Tian, J.; Zhu, S.; Dai, Y.; Qin, C. Fast Cone-Beam CT Image Reconstruction Using GPU Hardware. *J. X-Ray Sci. Technol.* **2008**, *16*, 225–234.
53. Paxino, G.; Watson, C. *The Rat Brain in Stereotaxic Coordinates*; Elsevier: New York, 2006.